



PAPER • OPEN ACCESS

A highly scalable and autonomous spectroscopic radiation mapping system with resilient IoT detector units for dosimetry, safety and security

To cite this article: Frederick S Russell-Pavier *et al* 2023 *J. Radiol. Prot.* **43** 011503

View the [article online](#) for updates and enhancements.

You may also like

- [Assessment of a localized deterministic spatial interpolation method in generating an indoor radiofrequency radiation map](#)
John Paul O. Bustillo, Randy Joseph G. Fernandez and Herbert B. Domingo
- [Safecast: successful citizen-science for radiation measurement and communication after Fukushima](#)
Azby Brown, Pieter Franken, Sean Bonner et al.
- [Relationship between indoor ambient dose equivalent rates and the architectural style of standalone houses in locations with high naturally occurring radionuclide soil concentrations](#)
J A Corbacho, J García-Paniagua, A Baeza et al.



PAPER

OPEN ACCESS

RECEIVED
24 August 2022REVISED
2 November 2022ACCEPTED FOR PUBLICATION
13 December 2022PUBLISHED
13 January 2023

Original Content from this work may be used under the terms of the [Creative Commons Attribution 4.0 licence](#).

Any further distribution of this work must maintain attribution to the author(s) and the title of the work, journal citation and DOI.



A highly scalable and autonomous spectroscopic radiation mapping system with resilient IoT detector units for dosimetry, safety and security

Frederick S Russell-Pavier* , Suresh Kaluvan, David Megson-Smith, Dean T Connor, Samuel J Fearn, Euan L Connolly, Thomas B Scott and Peter G Martin 

Interface Analysis Centre, University of Bristol, Tyndall Avenue, Bristol BS8 1TL, United Kingdom

* Author to whom any correspondence should be addressed.

E-mail: freddie.russell-pavier@bristol.ac.uk

Keywords: contamination, monitoring, dispersion event, IoT, networks, RDD

Abstract

Technologies utilizing radiological materials across power generation, defence, industry, research and medicine have increased the global inventory of highly active and hazardous materials. Consequently, an amplified threat exists of illicitly obtained materials being used as part of hostile acts. The potential for intentional releases occurs alongside risks from natural disasters or facility accidents. In any such event, it is crucial to rapidly assess the release composition and extent of response and remediation activities. Therefore, the deployment of an effective, resilient and autonomous radiation monitoring network is pivotal both during and after an incident. Underpinning this assessment is a detailed understanding of the pre-event or background, radiation levels, the knowledge of which is also essential in assessing a population's dosimetric exposure to, and impact from anthropogenic and naturally occurring/varying sources of ionizing radiation. Presented here is a fully operational cloud-based spectroscopic radiation mapping platform comprising IoT modules compatible with cellular networks, without modification, in over 180 countries. Combined with locally roaming vehicles, a continuous multi-pass radiological characterization of an urban environment was performed. Such IoT devices are deployable as either individual sensors for specific localized temporal events or integrated over a greater time period (and area) to represent a larger static sensor. Over several months of continued operation, more than 1000 000 individual location-referenced gamma-ray spectra were collected and securely uploaded, in real-time, to an online cloud database and automatically characterized via a custom multi-step workflow. Fine-scale local variations in the radiological fingerprint of a 1 km × 1 km urban area were subsequently rendered in near-real-time to an interactive secure online graphical dashboard for temporal, spatial and spectral interrogation by the user. Considerations for the automated 'elastic' handling of ever-expanding volumes of input data have been carried out, facilitating propagation and expansion of the system's database without human input.

1. Introduction

The once small group of countries with well-managed and secure nuclear material inventories is being rapidly joined by dozens of other nations [1], many of whom have limited experience in the safe and secure operation and management of a nuclear fuel cycle, thereby increasing the potential for unauthorized access, subversion, theft and misuse of materials. Power reactors are not the only source of threat materials, with historic gamma irradiators and radiotherapy (teletherapy) devices, such as those used in medical and treatment facilities around the world, containing TBq quantities of isotopes, including Co-60, Ir-192 and Cs-137 [2]. While these systems have been almost entirely retired in developed countries, large numbers remain in developing countries—across Africa, Asia and Eastern Europe [3]. Industrial autoradiography is a further application of radioactive materials, with estimates that hundreds of PBq of material ($\sim 10^{18}$ Bq) is

globally distributed [2]—an inventory equivalent to many times that released from the Chernobyl Nuclear Power Plant during the 1986 accident and explosion [4, 5]. Although regulatory restrictions exist to protect these radioactive sources, frequent reports occur of legacy or ‘orphaned’ materials being discovered [6]. In the wrong hands, the dispersal of just one of the high-activity sources would be catastrophic—with the public and broadcasters often quick to draw extreme nuclear analogues [7].

Despite the global media frequently reporting on the activities of state-sponsored nuclear weapon programs, coverage is seldom afforded to the growing number of radioactive material thefts, unauthorized possession, and most alarmingly, the stated intentions of extremist groups to acquire and use radioactive materials for malicious acts. Whether from the nuclear fuel cycle or medical and industrial sources, these high-activity radioisotopes can be, and have been, used for malicious and harmful purposes—namely within radiological dispersion devices (RDDs), otherwise termed ‘dirty bombs’. Continued threat assessments from the UK’s Royal Society and British Government’s own CONTEST and PROTECT strategies increasingly highlight the UK as being ‘extremely vulnerable, ill-equipped, and a primary target’ for these easily fabricated weapons of mass economic, humanitarian, societal and infrastructure disruption [7]. Hence, the challenge is the production and delivery of a discrete, sensitive, efficient, economical, yet accurate, distributed radiological monitoring capability through which illicit gamma-ray emitting radioactive materials (carried on-person or in-vehicle) can be detected and the resulting threat eliminated. The most prominent and high-profile threat detection and screening system in the UK for gamma and/or neutron sources (with equivalents at ports around the world) is the AWE-managed ‘Programme Cyclamen’ [8, 9]. The multi-agency capability comprises a network of large-volume polyvinyl-toluene (PVT) scintillator-based radiological portal monitors (RPMs) through which traffic entering the UK passes, providing an initial radiation ‘trip-wire’. Due to their considerable active detection volume, while effective in identifying containers or vehicles requiring subsequent inspection, the poor spectroscopic performance of the PVT material in RPMs limits their ability to isotopically identify radionuclides. This results in a significant number of false-positive alarm activations, each necessitating expert review and assessment. Furthermore, their static nature results in the capability being unable to provide any time-resolved geospatial information on changing radiation levels or mapping capability, away from the limited number of locations at which they are installed.

Aside from the static port-based ‘Programme Cyclamen’ and a small number of site-specific systems, the UK’s other primary distributed monitoring provision for the detection of radioactive threat sources that could be used as part of an RDD attack is termed ‘SIGMA’, a translation from an analogous US DARPA programme of the same name [10]. Like analogous systems in other countries, the capability comprises a suite of considerably smaller portable detector devices installed around strategic locations or transported on-foot or in-vehicle by law-enforcement personnel. While the exact nature and specifics of both the software and hardware that comprise the platform are not fully disclosed, the resilient and secure assimilation, processing, inter-comparison and visualization of large volumes of location-specific, and typically noisy/poor-quality spectroscopic data from fleets of fixed and roaming radiation detectors represents a unique and complex challenge necessitating experienced operator input. Therefore, alongside a suite of hardware advancements, this study seeks to address these current limitations through a highly automated and intuitive approach, removing the requirement for expert users to critique, understand and evaluate the results.

The aforementioned systems attempt to detect the transit of illicit radioactive and nuclear materials, preventing their potential catastrophic release, in the aftermath of a nuclear incident or RDD attack. However, it is also crucial for the subsequent response and remediation phases that not only the resulting radiation is mapped, quantified and assessed, but also that the pre-event ‘normal’ of the now contaminated area is understood. It is only from an appreciation of this change or ‘delta’, in radiation signature (from what previously existed) that successful and cost-efficient remediation can occur. The absence of a suitable prior baseline for comparison has resulted in significant difficulties in remediation activities across the Fukushima-affected fallout zone [11, 12]. Consequently, a high spatial and temporal resolution understanding of the background radiation levels and signatures across towns, cities, regions, and even entire countries, is as essential for civic recovery following a radiological release event as it is for preventing such an attack.

The 2011 INES Level 7 accident at Japan’s Fukushima Daiichi Nuclear Power Plant (FDNPP) served to bring about a step-change in radiation mapping capability—enabled by the incorporation and assimilation of the best-available hardware and software at the time. One system to emerge was the Geiger–Muller tube-based Safecast suite of hardware, the most widely deployed of which is still the highly portable ‘bGeigie Nano’ [13]. In logging mode, the device writes, to an internal storage SD card, a radiation measurement every 5 s, alongside GPS-derived geospatial co-ordinates. This entire catalogue of data is subsequently uploaded by the user to the cloud for visualization and analysis through an associated mobile phone application. As well as being non-spectroscopic, and therefore unable to differentiate between radioisotopes,

and capturing measurements only once every 5 s, the reliance on the user to ‘push’ data to the cloud results in an appreciable post-capture delay. Hence, the data are not available, or displayed, in real time.

A further system born from the FDNPP accident was the Kyoto University RAdiation MApping system, or KURAMA, alongside the latter KURAMA-II and subsequent Ultra-Compact KURAMA-II [14–16]. Unlike the Safecast system, these platforms contain solid-state radiation detection modules capable of spectroscopic measurements, alongside a meshed radio-communication network and Global System for Mobile Communication (GSM) gateway for (near) real-time autonomous wireless data upload. While superior in functionality to the Safecast systems, the use of a scintillator-type radiation detector in the KURAMA platforms (among other more advanced hardware) results in a greater total platform cost of \$1000’s versus \$100’s. Although more advantageous than Safecast, limitations are still associated with the overall KURAMA system’s architecture, resilience, output compatibility and downstream processing, as well as big-data ‘warehousing’ (above those of Safecast). It is these shortcomings that this study seeks to remedy, through the implementation of advancements in Internet of Things (IoT) and cloud hardware and software, respectively.

The IoT and networks of distributed internet-enabled devices have become increasingly widespread in radiation detection applications [17–20] following the development of ever-capable and miniaturized microcontrollers and wireless communication technologies. Due to the low price-point of IoT hardware, it has become commonplace for vast IoT networks of sensors to be deployed, often presenting new research challenges [21]. These networks are often capable of producing overwhelmingly large and unwieldy data sets for a non-expert user, the result of which is delayed or impaired decision-making where the data are not communicated or presented effectively.

In order to provide a continuous, low-cost, high spatial and temporal resolution, resilient, and eminently scalable secure radiological ‘monitoring’ platform, this study seeks to implement the current ‘state-of-the-art’ technologies to develop the ‘Overwatch’ surveillance provision, offering live analysis on real-time spectroscopic data, simply rendered within an internet browser. Using Empirical Bayesian Kriging techniques, these data sets can be quickly used to generate maps of an urban environment in the cloud, with the underpinning data being intuitively interrogable by the user.

The ‘Overwatch’ radiation mapping units (RMUs) developed in this study are compact and can be used autonomously once powered. Through the use of IoT SIM cards, the units established internet connectivity and compatibility around the world (in more than 180 countries) without the need for any hardware or firmware reconfiguration. Using a combination of consumer off-the-shelf (COTS) hardware, including a microcontroller, single board computer (SBU) and USB power gamma-ray spectrometer, each mapper was capable of uploading one 12-bit gamma-ray energy spectrum once per 3 s period with appended meta-data, including device location and temperature.

RMUs published data messages online and these were concatenated into objects in the cloud. With the generation of each cloud object, event-driven analytics are run on the incoming data, with the results being made available in a database. Over the many months that this system has been operating, the database has become increasingly large. However, through the use of low-latency database querying, subsets of the data are rapidly rendered to a dashboard for display and subsequent user analysis.

2. Methods

In this study, a network of RMUs installed within vehicles that continually traversed an urban environment is presented, combined with an online visualization and analytic platform. Beyond powering and driving a vehicle, which in the UK requires a human driver to be present, no user intervention is required to collect, process or render live radiometric data into an interactive cloud-based radiation map. A set of fault resilient ‘black-box’ RMUs were created that would autonomously configure themselves, begin gamma-spectroscopy data collection and independently operate with spontaneous power-cycling that resulted from the highly varied nature of vehicle operation and short distance movements around an urban environment. To facilitate continuous spectroscopic monitoring within an urban environment through a network of vehicular-based IoT RMUs, a multi-layer software architecture is also necessary. This architecture requires the inclusion of microcontroller level firmware, sensor fusion software, communication transformations, databasing and geospatial rendering. All RMUs push the data collected to the cloud using a compressed parametric message format and a lightweight communication protocol. The arrival of each packet of new data triggers the generation of multiple parallel processing scripts that transform the data, making it available in an online database. A cloud-based map is then presented for a subset of the data containing 100 000’s of unique data points, where filtering, inspection and a simple analysis can be performed using an interactive secure online map viewer.

To provide adequate roaming measurement coverage over the region of interest (ROI) for this technology deployment trial, several University of Bristol (UoB) site vehicles that operate in and around the buildings in

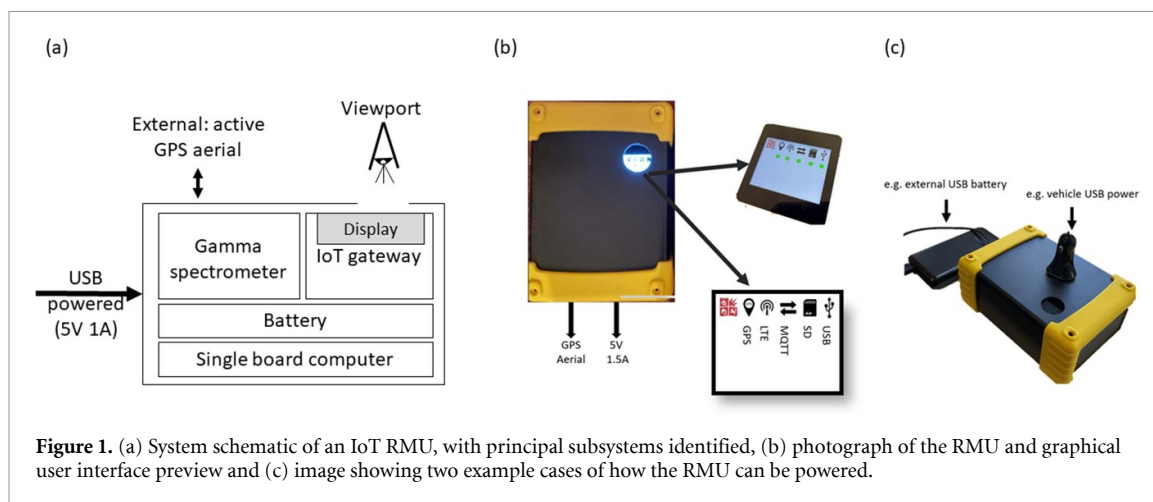


Figure 1. (a) System schematic of an IoT RMU, with principal subsystems identified, (b) photograph of the RMU and graphical user interface preview and (c) image showing two example cases of how the RMU can be powered.

its Clifton Precinct, with a nominal area of $1 \text{ km} \times 1 \text{ km}$, were chosen for their high number of repeated short journeys. These trips, in multiple vehicles, occurred almost continuously 24 h a day in all conditions, with roads traversed in both directions at a range of speeds. The complex and congested nature of such a built-up environment—with both GPS and GSM ‘black-spots’, alongside areas with considerable radio-frequency interference, served as a comprehensive test-bed for both the system’s subsequently detailed hardware and software components.

2.1. IoT RMUs

Each RMU has dimensions of less than $20 \text{ cm} \times 15 \text{ cm} \times 10 \text{ cm}$, and weighs 1.5 kg. To afford mechanical protection to the electronics within, an outer acrylonitrile butadiene styrene enclosure with a wall-thickness of 4 mm was selected. For testing, each unit was installed in the same location inside the patrolling UoB Security Services vehicle, underneath the front near-side passenger seat, resulting in a distance from the road surface of around $30 \pm 5 \text{ cm}$. From a ‘cold start’, i.e. powering on after a full power off, the device is able to boot-up, measure data and upload to the cloud within 60 s.

The maximum observed power consumption of each RMU is 5.5 W, therefore capable of being powered by typical consumer-grade USB power sources—including standalone battery packs, vehicle USB supplies, or even portable solar panels. In this deployment scenario, it is sufficient to rely solely on passive cooling of the boxes, as no extreme temperatures (e.g. $<0 \text{ }^\circ\text{C}$ or $>35 \text{ }^\circ\text{C}$) would be encountered when used inside the UoB’s site vehicles. However, where hot ($>40 \text{ }^\circ\text{C}$) or direct sunlight is incident onto the units, then active cooling is likely required for the device to function correctly. These hardware provisions would markedly increase the power requirements of the RMU by up to 50%, as well as requiring the application of the radiation detectors’ own temperature compensation for increased thermal noise within the module.

The RMU can be broken down into the following principal sub-components: gamma-ray spectrometer, IoT gateway, battery and single-board computer (SBC). Figure 1 shows a system schematic of an RMU. The gamma-ray spectrometer used in this study is the Hamamatsu Photonics C12137-01, comprising a CsI(Tl) scintillator crystal coupled to a multi-pixel photon counter and associated peak-shaping, processing and read-out electronics. The detector is directly interfaced with a standard Raspberry Pi 4 (4GB) SBC via USB 2.0. The same unit is also compatible with a range of other USB hand-held gamma-ray spectrometers through the Teams ‘Universal Detector library’, including those made by Kromek (e.g. GR1—a CdZnTe semiconductor-type device, and the SIGMA family of CsI(Tl)-based scintillator detectors). To permit the derivation of dose rate from the Hamamatsu C12137-01 detectors, rather than presenting a detector-specific counts per second value, the Hamamatsu simulation-derived, detector specific, $G(E)$ function is utilized. Here, for each gamma-ray photon incident on, and subsequently processed by, the detector (quantified by its energy calibrated channel) is ascribed a dose (in pSv)—the summation of these individual dose contributions results in the dose rate presented.

The SBC is both responsible for monitoring the sensors on a device level to ensure they continually report data correctly and also for fusing all peripheral sensor inputs into a message before a compressed message is outputted to the IoT gateway, again via USB. Upon receiving messages, the IoT gateway reports on completed actions, and if a number of failed attempts are detected via the SBC, a number of commands are sent from the SBC to the IoT gateway to re-initialize subsystems, including GPS, LTE, RTC or SD buffering. This additional layer of autonomous fault monitoring in the hardware allows the RMU to regularly cross-examine its functioning subsystem and be recoverable from a number of complex real-world scenarios

that occur when operating an RMU through areas of varying cellular, GPS signal and powering conditions, without the need for any user input.

This IoT gateway comprises a dual-core ESP32-based M5Stack Core 2 with integrated SIM7600G multi-band cellular module to provide internet connectivity. Carrier-agnostic, IoT-specific SIM cards supplied by EMnify are used in the IoT gateway sub-module. A key advantage of these SIM cards is their ability to make autonomous connections to over 540 cellular networks in more than 180 countries—switching between networks automatically, depending upon signal strength, without the need to manually reconfigure the cellular module or replace the physical SIM card. The IoT gateway screen provides additional metadata, including cellular signal strength, GPS status, real-time clock timestamp and a unique device identifier—each of which is appended to a message containing gamma-ray spectra, before the entire packet is pushed to the cloud using message queuing telemetry transport (MQTT) messaging. A summary of the status information is also displayed on the screen of the IoT gateway in the form of a traffic light style status indicator, so that the status of the device can be inspected at anytime by the user.

The IoT gateway also supports a computationally lightweight adaptive buffering method, using large onboard capacity and non-volatile SD cards (typically 32GB) as in remote locations, connectivity may be poor for several hours, or days, therefore generating a large backlog of data. This buffering solution is developed to be communication hardware agnostic, so that the IoT gateway can be readily adapted to use alternative communication methods, e.g. BLE, WiFi or LoRa. For every attempted data packet sent, a determination of communication integrity (i.e. cellular signal) is carried out by the IoT gateway, to ensure that in areas of poor signal the message will be flagged as requiring a subsequent message upload attempt while in a confirmed area of consistently high communication integrity, or signal strength. This approach facilitates improved data resilience in cases where an empty, partial or corrupted form message can be delivered to the intended IoT endpoint, generating subsequent issues within the data pipeline. In summary, this custom methodology was developed for a number of application-specific reasons, including the following:

- **Maintenance of operational functionality**—preserving the low-level ability for communication between hardware to be agnostic, e.g. LoRa and other mesh-type network architectures.
- **Deployment uncertainties**—due to the high likelihood of IoT devices being sporadically power-cycled or broken while in the field, a robust architecture is necessary to ensure that data are still recoverable/stored, even if power and/or communication connectivity are lost. Consequently, the non-volatile memory on the SD card is utilized, which also permits the SD card to be removed from the system and inserted into a computer to provide a secondary means of uploading data to the cloud.
- **Data aggregation**—as units deployed in the field can operate for hours, if not days, without mobile (GSM) signal, the potential exists for large ‘backlogs’ of data waiting to be uploaded, to be generated. Since the available memory in the cellular module is far smaller than that of the SD card, the system was designed to minimize the opportunity for data loss by using the larger memory space contained within the SD card(s).

2.2. Cloud-based services

The SIM7600G cellular module possesses inbuilt support for the commonplace MQTT IoT messaging protocol, through which data is passed to the cloud. This MQTT protocol is used to publish messages to a given topic in the Amazon Web Services (AWS) IoT Core, accessible from any registered and certificated ‘things’. To facilitate future scalability and automation, all RMU devices communicate to the same AWS IoT Core topic—with a human-readable JSON-style message structure implemented. This flexible messaging structure permits data streams derived from other sensor types to be uploaded as well as for data tags to be readily appended to the message string, while still making use of the cloud upload and subsequent processing architectures. In addition, this message format avoids the data arriving from legacy modules becoming obsolete or incompatible with successive designs.

In every 60 s temporal window, all messages arriving at the IoT topic are concatenated into a file via automated data processing using AWS Kinesis, before being passed to an online storage ‘bucket’ using AWS S3. For each file created in this online storage environment, a cloud-based python script is triggered using AWS Lambda. This script, comprising a number of functions, performs data transformations, such as uncompressing the spectra, converting the gamma-spectrometer energy bin array to photon energy using a detector calibration function, deriving dose rates via the aforementioned detector-specific $G(E)$ function, alongside undertaking gamma-ray peak identification for known emitters via a Python module previously developed by the team, herein deployed on the cloud rather than locally [22]. Once the data is transformed, it is made available in a database. Resulting from the flexibility and scalability afforded by the AWS cloud provisioning, the processing ‘workflow’ can be easily manipulated and iterated, depending on the system requirements and hardware changes as shown in figure 2.

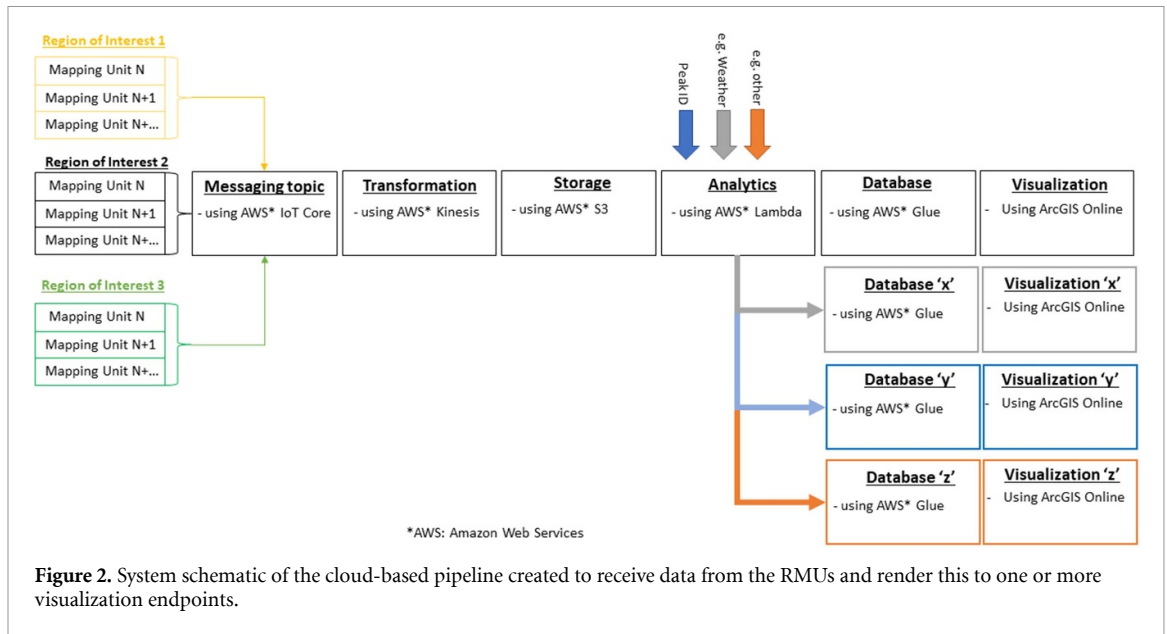


Figure 2. System schematic of the cloud-based pipeline created to receive data from the RMUs and render this to one or more visualization endpoints.

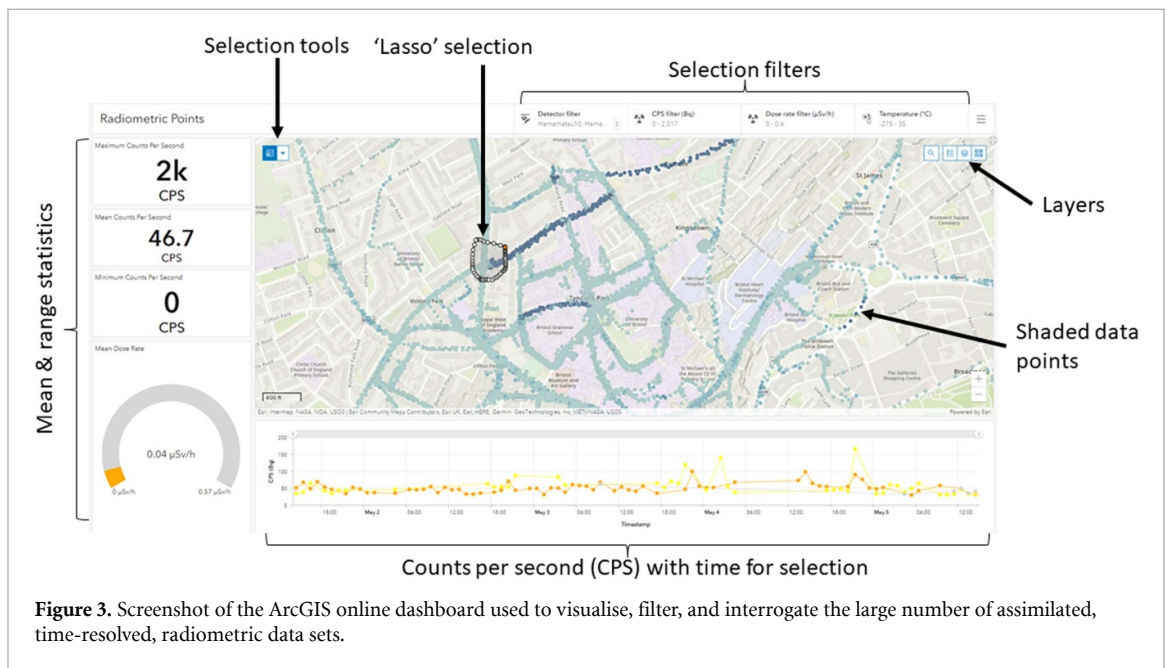


Figure 3. Screenshot of the ArcGIS online dashboard used to visualise, filter, and interrogate the large number of assimilated, time-resolved, radiometric data sets.

2.3. Data visualisation, inspection and analysis

Detailed analysis and visualization of large geospatial data sets is performed using a range of services within ArcGIS Online. The geospatial data is automatically imported into the environment on a time-scheduled ArcGIS online notebook before being rendered onto an interactive map and feature service. Alongside colour shadings to signify dose-rate variations, further feature layers with additional classification of the data are generated for regional analysis—such as identifying localized regions of higher activity, interpolation or temporal trends. Figure 3 presents an overview of the ArcGIS online dashboard for data visualization and inspection that renders the feature service and associated data. A further benefit of using ArcGIS online for this application, is the flexibility and security of a given ArcGIS online dashboard to be accessible only within a specified domain or for certain users, as well as permitting dashboards to be made publicly accessible—therefore catering for a number of possible real-world scenarios where this architecture could be deployed.

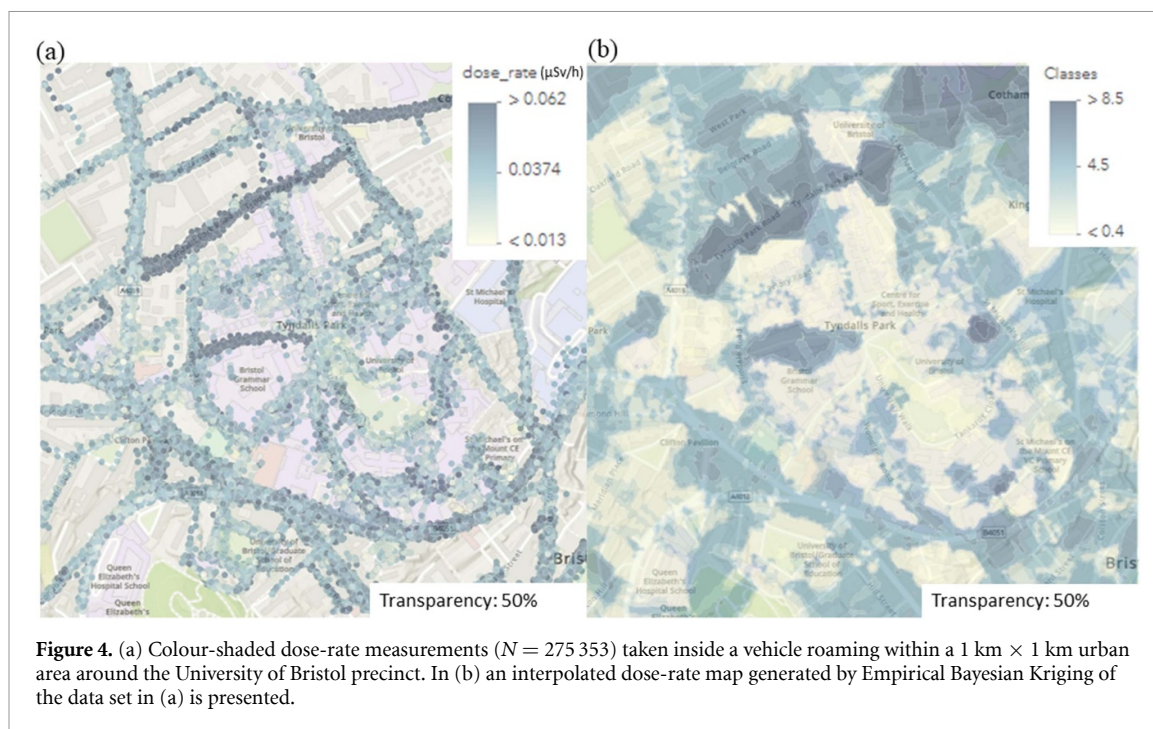


Figure 4. (a) Colour-shaded dose-rate measurements ($N = 275\,353$) taken inside a vehicle roaming within a $1\text{ km} \times 1\text{ km}$ urban area around the University of Bristol precinct. In (b) an interpolated dose-rate map generated by Empirical Bayesian Kriging of the data set in (a) is presented.

3. Results

The primary aim of this trial deployment of RMUs is to evaluate the complete system across an uncharacterized and continually evolving real-world environment—demonstrating the capability for autonomous and continuous real-time radiological mapping without the need for user input for data to be assimilated and user-interrogable. During the time period between 30 January 2022 and 30 June 2022, a network of eight RMU devices collected a total of 1368 175 gamma-ray spectra around Bristol, with a mean exposure time of $3.2 \pm 0.1\text{ s}$. This resulted in a total number of gamma-ray detection events of 1.31×10^8 , distributed over an area of $1 \times 10^6\text{ m}^2$. The overall mean dose rate measured inside a vehicle within the area studied was found to be $0.0376\ \mu\text{Sv h}^{-1}$, with the dose rates on some roads observed to be in excess of ten times higher than this mean dose-rate value.

A summary of the dose-rate variation seen across the RoI is presented in figure 4. The data in figure 4 is a 38 d sub-selection of the total data, corresponding to 275 353 data points to allow for enhanced visualization performance online, collected by vehicles carrying RMUs across the $1\text{ km} \times 1\text{ km}$ RoI between 4 April 2022 and 11 May 2022. Two means of visualization are shown. First, via an interpolated map, generated using the Empirical Bayesian Kriging tool provided by the online toolset within ArcGIS, and second, the underlying shaded data points collected by the RMUs. The uncertainty associated with the use of Empirical Bayesian Kriging is presented in figure 5 [23].

Additional hot- and cold-spot identification, within the context of low-level background radiation, can be determined by calculating the Getis-Ord G_i^* statistic for each feature. This statistical measurement not only calculates the z-scores (number of standard deviations from the mean) and associated p-values (probability) for each data point, but it evaluates whether the cluster of data points is significantly different from the expected value for that cluster as predicted using the entire data set. Visualizing the Getis-Ord G_i^* statistic was found to provide an intuitive means by which to examine the subtle variations that exist between the background dose rates in densely packed geospatial data, within the bounds of such an urban area [24]. Figure 6 highlights such a distribution—with regions of both high and low dose rates across the RoI appearing to not only be clustered in isolated areas, but to exist around specific road sections—with activity levels being significantly higher for certain stretches than adjoining, or neighbouring, roads. A second, smaller RoI $250\text{ m wide} \times 700\text{ m high}$, labelled Region A.1 in figure 6, was chosen for further analysis. In RoI A.1, there exist four parallel roads with contrasting statistical variation. Sections from four roads: Belgrave, Tyndall's Park (TPR), Priory (PR) and Elton, ranging between 170 and 230 m in length, are compared in figure 7(a). The dose-rate mean and the standard deviation are subsequently presented in figure 7(b), with the cumulative gamma-ray spectra from a sample of 500 points from each road presented for comparison in figure 7(c) to illustrate the contrasting gamma-ray spectra between each of the roads.

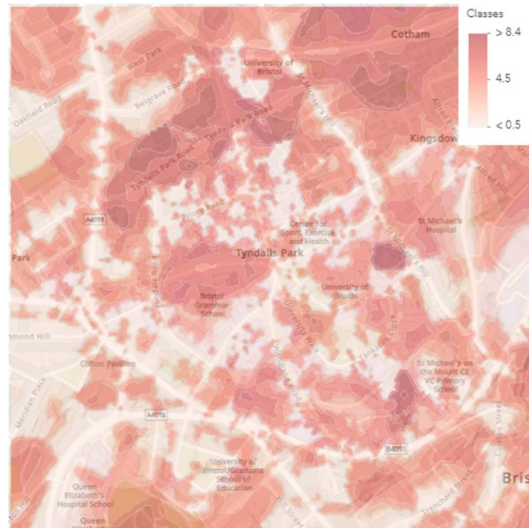


Figure 5. Predicted error (colour-shaded) of the interpolated radiation map generated via Empirical Bayesian Kriging using data collected via road over the 1 km × 1 km urban area.



Figure 6. Hot- and cold-spot dose-rate localities identified using the Getis-Ord G_i^* statistic for each of the data points across the RoI.

Detailed inspection of the data collected on TPR, the highest dose-rate road, was performed to ensure the network of multiple RMUs provided consistent data. Due to the vehicle activity undertaken on this road, it was possible to compare the results acquired from two RMUs over a 38 d period. During this time, the first RMU carrying ‘Hamamatsu 3’ (H3) passed through TPR a total of 127 times (collecting 571 spectra), and the second IoT-RMU, carrying ‘Hamamatsu 10’ (H10), passed through TPR 89 times (collecting 457 spectra). In figure 8(a), a dose-rate radiation profile alongside latitude is presented for the two detection units. The two systems showed consistent agreement with the mean for H3 at $0.229 \pm 0.025 \mu\text{Sv h}^{-1}$, whereas for H10 it was found to be $0.236 \pm 0.027 \mu\text{Sv h}^{-1}$. The RMS error between the two RMUs is therefore minimal, at $0.0348 \mu\text{Sv h}^{-1}$.

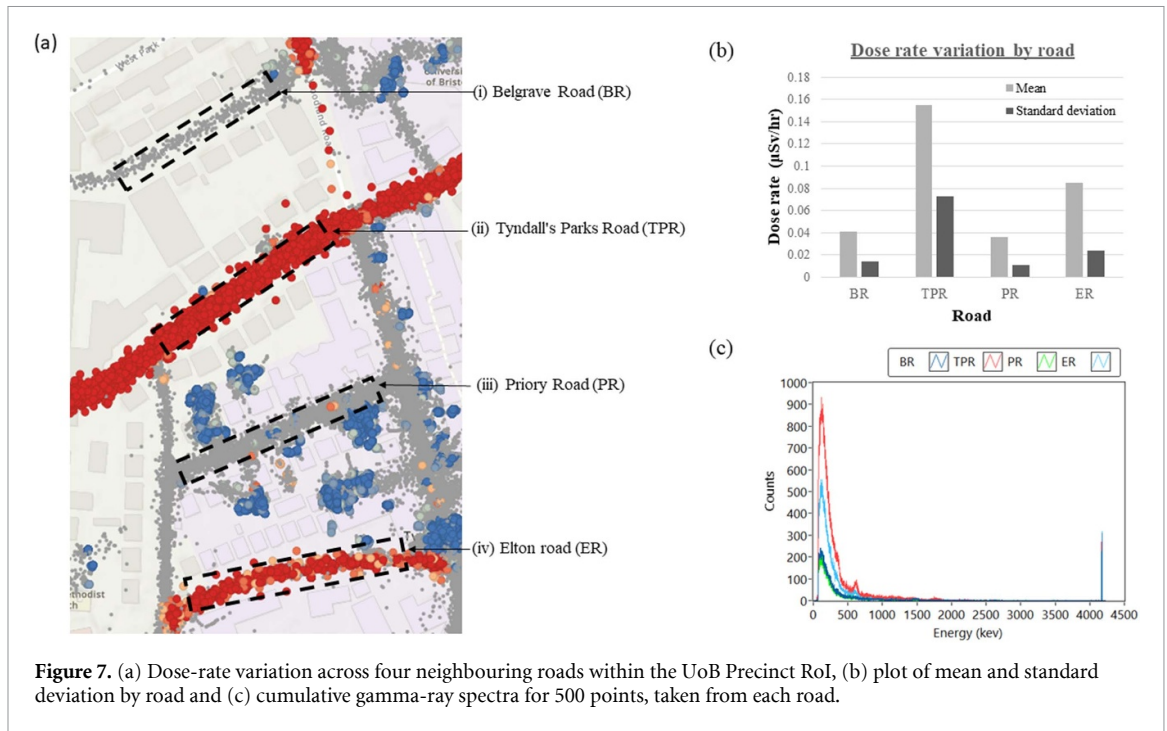


Figure 7. (a) Dose-rate variation across four neighbouring roads within the UoB Precinct RoI, (b) plot of mean and standard deviation by road and (c) cumulative gamma-ray spectra for 500 points, taken from each road.

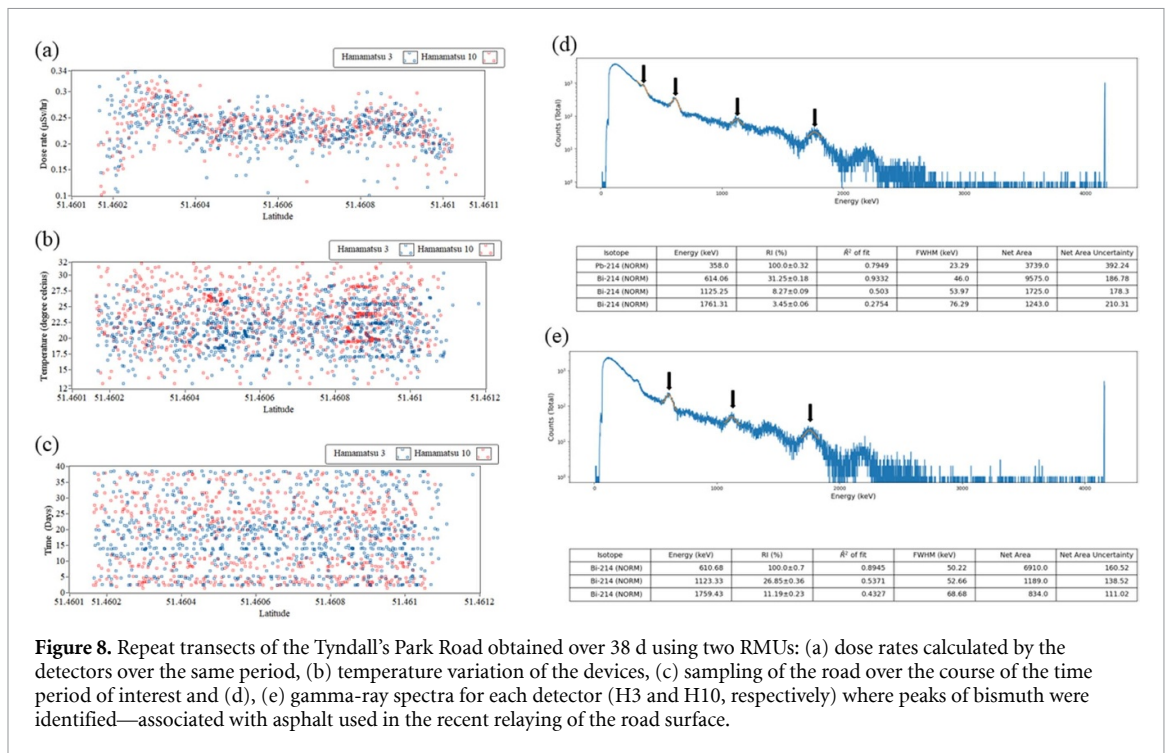


Figure 8. Repeat transects of the Tyndall's Park Road obtained over 38 d using two RMUs: (a) dose rates calculated by the detectors over the same period, (b) temperature variation of the devices, (c) sampling of the road over the course of the time period of interest and (d), (e) gamma-ray spectra for each detector (H3 and H10, respectively) where peaks of bismuth were identified—associated with asphalt used in the recent relaying of the road surface.

From figure 8(b), the detector temperature variation is shown to be in the range of 12 °C–32 °C, with the mean for H3 at 21.4 ± 3.2 °C and H10 at 22.8 ± 3.7 °C. The data sampling from each RMU was similarly distributed across the time-frame of interest, as can be seen in figure 8(c), making them suitable candidates for comparison. As per the online workflow, the cumulative spectra collected by each RMU were automatically passed through the isotopic peak ID fitting software [22], where three prominent peaks associated with bismuth-214 (in both cases) and lead-214 (in the H3 cumulative spectrum) were identified. The results presented in figure 8 depict strong agreement in the characterization of TPR through the 38 d window, and also show that elemental peak analysis can be performed ‘online’ (in workflow) from the RMU data, while mounted inside and transiting within a vehicle.

4. Discussion

The initial study carried out with IoT RMUs showed operational success for both the devices and the scalable software architecture, as the devices continued to function without human interaction for many months, with user error (physically unplugging the devices) being the only cause of data not being captured. However, upon re-insertion into the vehicles' USB power supply, data collection resumed without the requirement for intervention.

A significant observation, verified by multiple passes using multiple detector RMUs, is the presence of high levels of variation in background radiation across otherwise visually homogeneous roads within an urban environment. By comparison, TPR was observed to possess a mean dose rate of $0.165 \mu\text{Sv h}^{-1}$, with a maximum of $0.571 \mu\text{Sv h}^{-1}$ (samples = 390), compared with an adjacent road, PR, with a comparable dose rate of $0.0301 \mu\text{Sv h}^{-1}$ (samples = 805) and a maximum of $0.0663 \mu\text{Sv h}^{-1}$. However, this variation represents only a snippet of the complex radiation profile present within a typical urban environment. Where these variations occur, they appear to stop at the intersection with another road, supporting the hypothesis that the variations observed are dominated by road surface/tarmac dressing contributions, as the resurfacing of roads is likely to happen road-by-road over a period of months, if not years. Furthermore, urban environments are indefinitely prone to change with ongoing developments of, or repairs to, civil infrastructure, clearly demonstrating that the use of a fixed anomaly threshold (in either energy specific or total detection events) to identify radiation abnormalities with mobile RMU is not appropriate and that more advanced outlier detection based on a continuously evolving model is required. Additional spectral analysis, based on anthropogenic perturbation of secular equilibrium, would allow for the timing of these civil works to be identified.

It is commonly discussed that radiation emissions from a given environment can be examined and quantified using static or roaming radiation monitors or a combination of both methods. From the data collected in this study, it is possible to see that (even in an arbitrarily urban environment with low levels of radiation) spatially close regions of a built-up urban area can be highly contrasting. With this in mind, a number of practical benefits have been experienced by a distributed network of roaming IoT RMUs, including the cross-checking and fault detection of detectors passing through the same area, both wide-scale and densely sampled measurement coverage with relatively few detectors, and higher statistical confidence in the resultant data set due to the same environment being characterized by multiple sensors. However, a notable disadvantage with a small number of roaming IoT RMUs is the downtime when the vehicle is not in active service and stationary (e.g. in a parking bay) in an arbitrary location, which may not yield useful data. Given the very low power requirements (i.e. $<5.5 \text{ W}$) of the RMUs developed in this study and the potential for the inclusion of other additional sensor types as part of the architecture, it is feasible to run in the vehicles strategically placed static sensors when the vehicles are not roaming.

While IoT RMUs were vehicle-mounted during the data presented here, the lightweight and low-powered systems are eminently transferable to other surveying modes, such as walking or robot-mounted usage. Using the touch screen user interface, the RMUs can be easily switched to different surveying modes and the associated data field changed for subsequent data uploads.

In addition to the regionally bounded data presented here, the RMUs have been successfully deployed outside of the UK (USA, Ukraine, France) without modification to the hardware or need for further user input—with data seamlessly arriving into the AWS 'S3 Bucket' and being visualized on the same cloud-based dashboard, giving promise to the technology being transferable and widely applicable.

5. Conclusion and future work

The development and deployment of a distributed network of low-cost IoT gamma-ray spectrometers continually traversing a city has revealed high levels of contrast across a relatively localized area of $1 \text{ km} \times 1 \text{ km}$. Due to the high uptime of a small number of roaming vehicles, it has been shown that a large geospatial data set can be gathered over a comparatively short duration of only a couple of months. Automatic post-processing and visualization in the cloud allowed for rapid analysis—affording an evolving representation of the background levels of radiation in an urban environment. A detailed and comprehensive study of a subsection of the RoI has highlighted that varied construction materials used in civil infrastructure containing radiogenic Bi-214 and Pb-214 can contribute to varied and complex distributions of dose rates between roads situated only 10s to 100s of metres apart. While the aforementioned radioisotopes have been directly identified in the gamma-ray spectra in areas with elevated background radiation, naturally occurring sources of uranium and radium are also likely to exist in the building materials used, and vary according to

their source. By building an accurate and continuous picture of the varied and evolving background radiation makeup in an urban environment, it is predicted that a more sensitive anomaly and threat detection algorithm can be implemented.

Future developments in the overall system will look to implement additional automated cloud-based analysis on the incoming live data from all IoT RMUs, utilizing low-latency two-way communications, to pass any significant observations back to the IoT RMUs. This capability could facilitate advances such as informing roaming vehicles to nearby locations of interest for further investigation, for instance, due to significant change detection determined by a continually evolving multi-agent background model generated online. This two-way communication would allow for the 'Overwatch' system to develop capabilities to determine and inform the best strategy for resampling low-confidence or possible triggering areas, i.e. by suggesting vehicle route adjustments in real time. Due to the intermittent coverage experienced within the urban environment during field testing, it would also be expected that a simpler offline model of background radiation levels could be kept on the RMUs for the rapid comparative determination of anomalies.

Future work will also seek to deploy the full 'Overwatch' capability in one of the 180 GSM network-supported countries, to assist in the characterization of a situation where an evolving radiological scenario, e.g. due to a natural event or human activity that disperses radionuclides across an urban environment requiring subsequent characterization and decontamination procedures to occur. In this situation, utilizing vehicles, such as those used by emergency services that conduct many repeated journeys in a given RoI, would be desirable to give equivalent data density to that presented here. In such an event, where gamma-ray emitters are present on the road surface and can be mobilized by the vehicles' tyres or bodywork, causing a local elevation in detected radiation by a given RMU, future work would look to incorporate intelligence, using a multi-agent model, to detect instances of 'self-contamination' when roaming through a previously well-characterized environment.

With a reduction in the cost of more compact gamma-ray spectrometers, and with improved measurement sensitivity as portable technology improves, it is becoming ever more feasible that multiple RMUs could be installed in the same vehicle for in-phase or anti-phase analysis. An added advantage of multiple sensors being installed in the vehicle would include providing better directional sensitivity to a given roaming vehicle, and therefore better localization of abnormal radiation signatures.

Data availability statement

The data used in this study is freely available from the University of Bristol data repository, data.bris, at: <https://doi.org/10.5523/bris.1hqjys85s8e392qg3fmqkm2o0i>.

Acknowledgments

The authors acknowledge the financial support for this study provided by the University of Bristol's Policy Bristol Team, STFC-AWE funded Nuclear Security Network (NuSec) and Atomic Weapons Establishment (AWE). P G M acknowledges the funding provided by the Royal Academy of Engineering (RAEng) as part of his Research Fellowship. T B S acknowledges UK Research and Innovation, specifically the Engineering and Physical Sciences Research Council (EPSRC) for their funding via the Robotics and AI in Nuclear (RAIN) Project (EP/W001128/1). T B S also thanks the Royal Academy of Engineering for their direct funding via the academy Fellowships scheme. D T C acknowledges funding from the National Nuclear Laboratory (NNL) Core Science Decontamination Science Theme and UK Research and Innovation (UKRI) through the National Centre for Nuclear Robotics (NCNR) (EP/R02572X/1).

Jessica Wynne, Kathleen Smith, Peter Phillips and Addy Pope from ESRI are thanked for their assistance with the development of the outline ArcGIS Dashboard architecture and AWS integrations.

Conflict of interest

The authors declare no conflict of interest, financial or otherwise.

ORCID iDs

Frederick S Russell-Pavier  <https://orcid.org/0000-0002-2150-6989>

Peter G Martin  <https://orcid.org/0000-0003-3395-8656>

References

- [1] Alwaeli M and Mannheim V 2022 Investigation into the current state of nuclear energy and nuclear waste management—a state-of-the-art review *Energies* **15** 4275
- [2] United Nations Scientific Committee on the Effects of Atomic Radiation 2022 *Sources, Effects and Risks of Ionizing Radiation* (available at: www.unece.org/unscear/en/publications/2020_2021_1.html)
- [3] Kouzes R T 2005 Detecting illicit nuclear materials: the installation of radiological monitoring equipment in the united states and overseas is helping thwart nuclear terrorism *Am. Sci.* **93** 422–7
- [4] IAEA 2018 *Status and Trends in Spent Fuel and Radioactive Waste Management* (Vienna: IAEA)
- [5] International Atomic Energy Agency 2008 *Estimation of Global Inventories of Radioactive Waste and Other Radioactive Materials (IAEA TECDOC Series No. 1591)* (Vienna: International Atomic Energy Agency)
- [6] Dimitrovski D and Kittley S 2015 *Incident and trafficking database: new systems for reporting and accessing state information Technical Report* International Atomic Energy Agency
- [7] Brady E 2016 *An Analysis of the UK's Counter-Terrorism Strategy, Contest and the Challenges in Its Evaluation* (Frankfurt: Universitätsbibliothek Johann Christian Senckenberg)
- [8] Downes R J 2021 Alarming cargo: regulation and control at the UK border *Terror. Political Violence* **33** 549–71
- [9] Fehlau P and Eaton M J 1979 *Passive nuclear material detection in a personnel portal Technical Report* (Los Alamos, NM: Los Alamos National Lab. (LANL))
- [10] Defense Advanced Research Projects Agency *SIGMA* (available at: www.darpa.mil/program/sigma) (Accessed 24 June 2022)
- [11] Moreno T, Wallis S R, Kojima T and Gibbons W 2016 *The Geology of Japan* (London: Geological Society of London)
- [12] Omori Y, Hosoda M, Takahashi F, Sanada T, Hirao S, Ono K and Furukawa M 2020 Japanese population dose from natural radiation *J. Radiol. Prot.* **40** R99
- [13] Brown A, Franken P, Bonner S, Dolezal N and Moross J 2016 Safecast: successful citizen-science for radiation measurement and communication after fukushima *J. Radiol. Prot.* **36** S82
- [14] Tsuda S, Yoshida T, Tsutsumi M and Saito K 2015 Characteristics and verification of a car-borne survey system for dose rates in air: Kurama-II *J. Environ. Radioact.* **139** 260–5
- [15] Institute for Integrated Radiation and Kyoto University Nuclear Science *KURAMA* (available at: www.rii.kyoto-u.ac.jp/kurama/en/index.html) (Accessed 24 June 2022)
- [16] Institute for Integrated Radiation and Kyoto University Nuclear Science *Ultra-Compact KURAMA-II* (available at: www.rii.kyoto-u.ac.jp/kurama/en/kurama-micro.html) (Accessed 24 June 2022)
- [17] Muniraj M, Qureshi A R, Vijayakumar D, Viswanathan A and Bharathi N 2017 Geo tagged internet of things (IoT) device for radiation monitoring 2017 *Int. Conf. on Advances in Computing, Communications and Informatics (ICACCI)* (IEEE) pp 431–6
- [18] Abimanyu A et al 2020 Design of IoT-based radiation monitor area for nuclear and radiological emergency preparedness system in Yogyakarta nuclear area *J. Phys.: Conf. Ser.* **1428** 012050
- [19] Baena-Navarro R, Torres-Hoyos F, Uc-Rios C and Colmenares-Quintero R 2020 Design and assembly of an IoT-based device to determine the absorbed dose of gamma and UV radiation *Appl. Radiat. Isot.* **166** 109359
- [20] Ahmad M I, Rahim M H A, Nordin R, Mohamed F, Abu-Samah A and Abdullah N F 2021 Ionizing radiation monitoring technology at the verge of internet of things *Sensors* **21** 7629
- [21] Moore S J, Nugent C D, Zhang S and Cleland I 2020 IoT reliability: a review leading to 5 key research directions *CCF Trans. Pervasive Comput. Interact.* **2** 147–63
- [22] Fearn S J, Kaluvan S, Scott T B and Martin P G 2022 An open-source iterative python module for the automated identification of photopeaks in photon spectra *Radiation* **2** 193–214
- [23] Russell-Pavier F, Martin P, Connor D, Fearn S and Connolly E 2022 A highly scalable and autonomous spectroscopic radiation mapping system with resilient IoT detector units for dosimetry, safety, and security (available at: <https://doi.org/10.5523/bris.1hqjys85s8e392qg3fmqkm2o0i>)
- [24] Getis A and Ord J K 2010 The analysis of spatial association by use of distance statistics *Perspectives on Spatial Data Analysis* (Berlin: Springer) pp 127–45